Available online at www.sciencedirect.com

SciVerse ScienceDirect

Journal of the European Ceramic Society 32 (2012) 1491–1501

www.elsevier.com/locate/jeurceramsoc

Surface crack in tension or in bending – A reassessment of the Newman and Raju formula in respect to fracture toughness measurements in brittle materials

Stefan Strobl [a,b,*], Peter Supancic [a,b], Tanja Lube [a], Robert Danzer [a]

[a] *Institut für Struktur- und Funktionskeramik, Montanuniversitaet Leoben, Peter-, Tunner-Straße 5, A-8700 Leoben, Austria*[1]
[b] *Materials Center Leoben Forschung GmbH, Roseggerstraße 12, A-8700 Leoben, Austria*[d]

Received 30 September 2011; received in revised form 14 December 2011; accepted 7 January 2012
Available online 6 February 2012

Abstract

The Newman and Raju formula for the stress intensity factor of a semi-elliptical surface crack loaded in uniaxial tension or in bending has been developed about 30 years ago using an FE-analysis for several geometric parameters and fitting an empirical equation to the data points. The Poisson's ratio analyzed was 0.3.

In this paper a reassessment of the Newman and Raju formula is made, where all relevant geometric parameters of crack and specimen and the Poisson's ratio are considered. The deviations of the old formula from the new results are up to 21%, if the full range of Poisson's ratio is taken into account. Furthermore the influence of the crack-surface intersection angle is discussed.

The results of this work are important for more precise fracture toughness measurements in brittle materials and give a practical guidance for appropriate specimen preparation for fracture toughness measurements, which is also considered here.

Keywords: Semi elliptical surface crack; Stress intensity factor; SCF method; Fracture toughness; Poisson's ratio

1. Introduction

The majority of standardized fracture toughness testing methods for ceramics use bending beams, containing a crack as sharp as possible and a well-defined geometry. The fracture toughness K_c is determined by application of the Griffith/Irwin failure criterion:

$$K_{Ic} \geq K = \sigma Y \sqrt{a\pi} \tag{1}$$

K_{Ic} is the mode I fracture toughness, K is the stress intensity factor (SIF), σ is a representative stress in the uncracked specimen (e.g. stress at the outer fibre at fracture), a the size of the crack and Y is a geometric factor, which is determined by the geometry of the specimen, the crack shape and the course of the stress field. For details see standard text books on fracture mechanics or on mechanical properties of ceramics.[1–3] Information on geometric factors for typical loading cases and standard specimen geometries can be found in literature.[4]

The Newman and Raju formula (NRF) is commonly used in the "Surface Crack in Flexure" (SCF)-method to determine fracture toughness in brittle materials. For materials with the Poisson's ratio $\nu = 0.3$, Newman and Raju (NR) [5] have developed a parameterized and generalized solution (i.e. fitting function) of the geometric factor $Y = Y\ (a,c,t,b,\phi)$ of a semi-elliptical surface crack in the stress field of a uniaxial tensile loaded or bended bar (thickness t and width $2b$). Therefore, Y depends on the geometry of the crack (crack width $2c$, crack depth a), the bar's cross-section and on the position at the crack front given by the crack angle ϕ, see Fig. 1.

Of course, fracture is initiated at the position the largest SIF along the crack front. But there exists some shortcomings which may conflict the exact determination of SIF and fracture toughness: Thirty years ago computer capacity was very limited which made a relatively coarse mesh necessary. Therefore the

* Corresponding author at: Institut für Struktur- und Funktionskeramik, Montanuniversitaet Leoben, Peter-Tunner-Straße 5, A-8700 Leoben, Austria.
Tel.: +43 3842 402 4113; fax: +43 3842 402 4102.
E-mail address: stefan.strobl@mcl.at (S. Strobl).
[c] www.isfk.at.
[d] www.mcl.at.

0955-2219/$ – see front matter © 2012 Elsevier Ltd. All rights reserved.
doi:10.1016/j.jeurceramsoc.2012.01.011

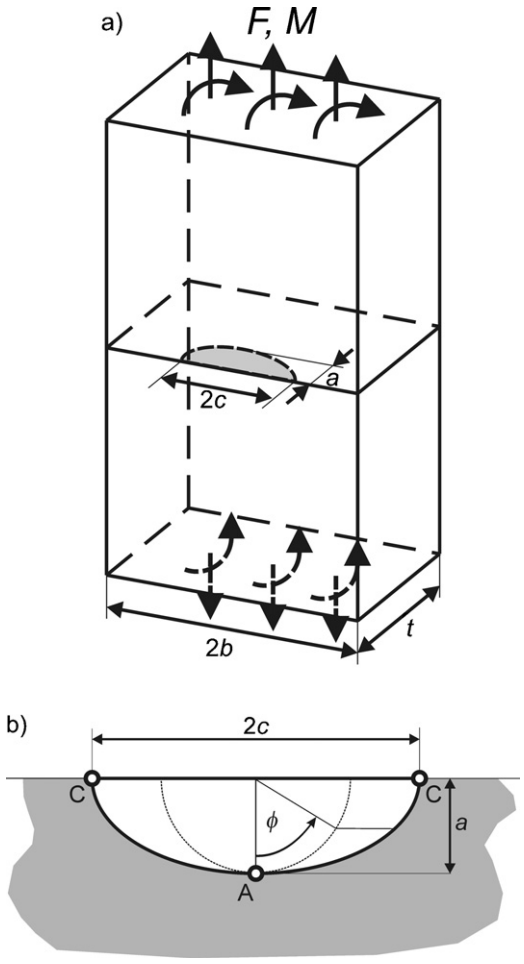

Fig. 1. (a) Schematic of a pre-cracked beam (loaded by normal force F or moment M) and (b) detail of the semi-elliptical crack assumed for the NRF. The crack width $2c$ at the surface and the crack depth a are indicated as well as the points A ($\phi = 0°$) and C ($\phi = 90°$), where the geometric factor Y can reach a maximum in the NRF.

precision of the analysis was not very high. (NR) specified their FE accuracy with ±3% compared to the analytical solution in terms of a completely embedded circular crack.[6,7]

In addition, to keep the fitting function simple, it cannot be very precise for all possible values of geometric parameters. NR claim that their provided fitting function has a maximum error of ±5% (related to the maximum of Y along the crack front) according to their FE results.[5]

Secondly, the analysis was only made for materials having the Poisson's ratio $\nu = 0.3$ which is the typical value of steels. This is also a good approximation for many engineering material classes. However, there are also many other materials – e.g. ceramics for structural applications or hard coatings – with a significant deviation regarding this value.[2,8–10]: Diamond (0.07), titanium diboride (0.1), zirconium diboride (0.14), glass and silicon carbide (0.16), hard metal and alumina (0.2), titan (0.36) or PMMA (0.4). Because even structural ceramics can deviate substantially, the Poisson's ratio should be considered in the data evaluation. In the literature, some calculations for an individual set of parameters can be found, e.g. by Isida et al. [4,11] in 1983, where for a special crack geometry data for several different Poisson's ratios are tabulated. But there is no general solution available.

Finally, the geometry of surface cracks used for fracture toughness measurements is – in general – not semi elliptical (the crack-surface intersection angle differs from 90°) which may result in additional uncertainties. This topic is treated in [12–15] in detail and addressed in.[16,17] A specific example has been studied by Fett.[18] For a crack, with the shape of circle segment, the differences to the semi-elliptical crack in the geometric factors are less than: ±7% in point A and less than ±2% in point C (see Fig. 1) for cracks having the same aspect ratio a/c. These results also are made for a specific case and their accuracy is unknown. The influence of crack-surface intersection angle will be investigated in detail in this work.

For these reasons, a reassessment of the NRF and a new fitting equation for the SIF is made in this paper. Semi elliptical cracks and cracks having a geometry, which is more relevant for fracture toughness testing of brittle materials, are considered. All results and the new fitting equation for the SIF are given at our home page (www.isfk.at/de/1006/) as an interactive WebMathematica tool. It is shown that – for realistic testing geometries – the NRF may result in huge deviations of the correct value in point A (up to 40% for $\nu = 0.3$).

Another aspect in SCF testing arises from the fact that – depending on the crack geometry and the Poisson's ratio – fracture can start at the deepest position of the crack (point A) or at its intersection with the specimen's surface (point C). The SCF analysis is valid for experiments with fracture origins at point A, while experiments with origins at point C are invalid for several reasons. In the last part of this paper parameter regimes are defined, where valid SCF-tests with origins at point A can be guarantied.

2. Methodology – FE model and parameters

The geometric factor Y for a surface crack having the geometry of an ellipse segment was determined in a parametric study for tension and bending loading (each 3125 FE runs). The results were used to define an interpolation function for Y. The considered parameter intervals are given in Table 1.

Characteristic parameters in our model are the crack depth a and its length at the surface c. Note that the crack intersects the surface with the angle χ (see Fig. 2), since the crack has the shape of a segment. The midpoint of the (truncated) ellipse is Δt ahead of the surface. It holds:

$$a_0 = \frac{a(a\cos(-\chi) + c\sin(-\chi))}{2a\cos(-\chi) + c\sin(-\chi)} \tag{2}$$

and

$$\Delta t = a_0 - a \tag{3}$$

The other semi-axis c_0 can be derived using the ellipse equation. Eq. (2) shows that for the crack shape ratio with the highest analyzed axis ratio ($a/c = 1.2$) the intersection angle of the semi-ellipse segment is $\chi \geq 70°$. This determines the lower limit for the parametric FE-study. Lower angles, which were possibly

Table 1
Parameter and considered parameter intervals for the realized FE study. For each parameter five equidistant design points have been used. For a/t the values 0.01, 0.05, 0.1, 0.3 and 0.5 have been chosen.

Dimensionless parameter name	Symbol	Lower limit	Upper limit
Rel. crack depth	a/t	0.01	0.5
Crack aspect ratio	a/c	0.4	1.2
Rel. crack width	c/b	0.1	0.5
Poisson's ratio	ν	0	0.4
Crack-surface intersection angle	χ	70°	110°

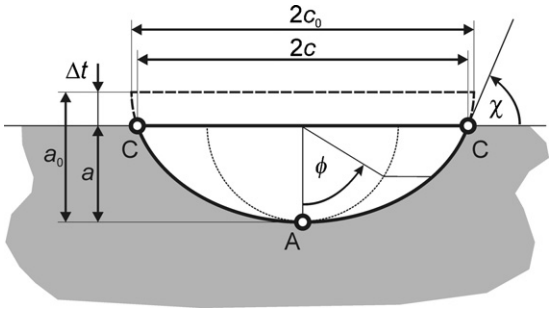

Fig. 2. Geometry of a surface crack (depth a, width $2c$) having the shape of an ellipse segment. Also the intersection angle χ is defined. The semi axes of the ellipse are: a_0, c_0.

needed, have been extrapolated and checked by some specific FE runs.

The computation of stress distribution in the specimen was performed in ANSYS Mechanical APDL Version 13.0. The quarter-model of the bar includes about 16,000 to 60,000 brick-elements (i.e. SOLID186).

The J-Integral method[19,20] – with quarter node collapsed crack tip elements (CTE) – was used to calculate the SIF. This well-implemented state-of-the-art method provides accurate results (the error is less than 0.01% compared to the analytical solution in the case of a fully embedded circular crack in pure tension).[19] Due to the CTE and the resulting ansatz functions, the crack tip singularity exponent is given with −0.5. Generally, this exponent deviates from this value if there is some influence of boundaries (e.g. at the free surface or near interfaces). So the SIF results are the "best fit" of the actual stress field with K as (FE internal) fit coefficient.

For all crack sizes, 30 elements along the crack front have been used and their alignment around the crack tip was equal. This was realized with an all hexahedron-meshed parallelepiped. Crack mesh details for different crack geometries are pointed out in Fig. 3, where three special cases are given exemplarily. The SIF was evaluated at all 61 nodes (including mid nodes) along the crack front.

In every case, singularity elements (CTE) along the crack front and a plain strain assumption (effective Young's modulus $E^* = E/(1-\nu^2)$) were deployed for the determination of the stress intensity, more precisely with the formulation $K = \sqrt{E^* \cdot J}$.

This approach is commonly accepted (e.g. see [19,21]), although generally plain stress state should occur at the surface. However, Zúñiga et al. [22] claim that the stress distribution at the surface can

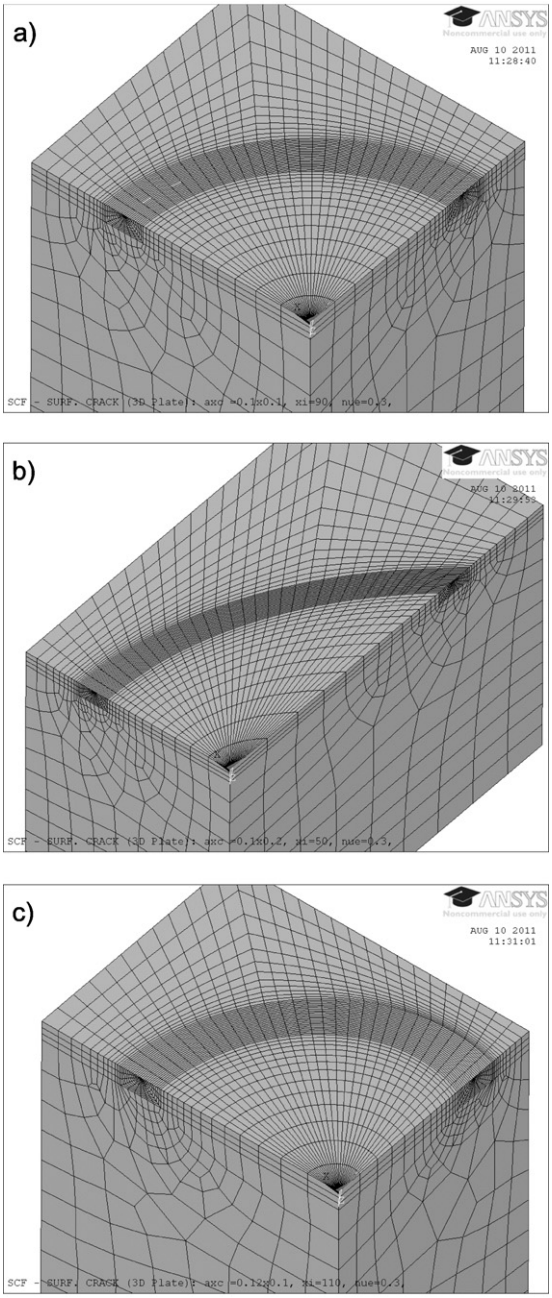

Fig. 3. Three examples of crack geometries and meshing details near the crack front. (a) $a/c = 1$ and $\chi = 90°$, (b) $a/c = 0.5$ and $\chi = 50°$, (c) $a/c = 1.2$ and $\chi = 110°$.

significantly deviate from the plain stress assumption in a 3D-geometry with crack. In addition, since the resulting K-values are always higher for plain strain, the calculation of the SIF at the region very close to the surface is a good approximation regarding safety aspects (e.g. for fatigue or proof of safety calculations).

Correlated to Eq. (1) the geometric factor along the crack front can be expressed with the related K, the nominal crack opening stress σ (i.e. 1 MPa) and the crack depth a (Note: Y always refers to the crack depth a, what means that a is taken as the typical defect size).

3. Results

The FE results and their tendencies behave, of course, similar to the generalized solution of NR.[5] For this reason this work has a focus on the main differences to the NRF and on the influence of the Poisson's ratio and the crack-surface interaction angle on the geometric factor. Since these effects are more pronounced for bending than for uniaxial tension loading all further results are plotted for $\chi = 90°$, c/b=0.1 and the bending case, if not specified else wise.

In Fig. 4 the current FE results (lines) are shown as a function of ϕ (the ratio a/t is parameter of the curves) for a semi-circular crack and are compared with the fitting solution of NR (plotted as points). The values of $a/t = 0$ are extrapolated (the last design point is at 0.01) and represent an infinitesimal small crack. This also eases the comparison with other publications, e.g. NR.

As expected, both results are nearly identical for $\nu = 0.3$ (Fig. 4a). Obvious deviations just occur for higher relative crack sizes as well as around $\phi \simeq 85°$. The last observation results from the facts, that the free surface influences the SIF (see also Section 4.3) and that there was no design point (i.e. node) in the calculation of NR. In other words their mesh was too coarse for such a detailed analysis.[6,7] For $\phi = 90°$ the agreement is good, since a design point for NR is there.

For $\nu = 0$ (see Fig. 4b) the results consequently shift compared to the NRF. This indicates that the Poisson's ratio has a significant influence on SIF. On the other hand there is no change in course of Y in the vicinity of $\phi = 90°$. The effect of the free surface is reduced since the Poisson's ratio decreases to zero.

In Fig. 4 two "exact" reference data points of Y for $\nu = 0$ and 0.3 published by Isida et al. [11] are marked. They showed that their method has an error less than 0.1%, which can also be shown with the method by Fett[23]. The results are tabled for an infinite plate (pure tension loading). Their obtained values of 0.659 and 0.036, respectively, are in excellent agreement with the present work: for $\nu = 0.3$ (see Fig. 4a) the extrapolated values of the interpolation function are 0.660 (tension) and 0.659 (bending). For $\nu = 0$ (see Fig. 4b) they are 0.635 (tension) and 0.636 (bending). Of course both loading cases should be equal in an infinite plate.

For shallow cracks ($a/c = 0.4$) an analogue comparison is illustrated in Fig. 5. The results in point A and C match the NRF quite good for $\nu = 0.3$ (Fig. 5a). Large deviations arise just in between these points, especially for small relative crack sizes (max. 12% at $\phi \approx 60°$). The results obtained for $\nu = 0$ (Fig. 5b) confirm the same down-shifting trend as for semi-circular cracks. This results in high average deviations.

In the following, the influence of the Poisson's ratio is investigated in more detail. As anticipated, the curves respecting semi-circles and $\nu = 0.3$ correlate well with the fit of NR (Fig. 6a). Inside the specimen the geometric factor increases (much stronger than linear) with increasing Poisson's ratio, but near the surface the effect is contrary; Y declines for higher Poisson's ratios. The same non linear trends can be observed for small crack shape ratios a/c, see Fig. 6b.

The influence of the crack-surface intersection angle χ on the SIF is very pronounced (along the whole crack front; see Fig. 7). In both cases, semicircular and shallow crack, χ influences the SIF even at the deepest point of the crack (A), although the characteristic crack parameters a and c (only these both are normally used to characterise the crack) are kept constant and the crack front has almost the same curvature in point A. Here the SIF and Y, respectively, decline with decreasing χ. In point C the influence of χ is very strong compared with point A. The magnitude of this effect has to be observed skeptically. For instance, the J-Integral evaluation is valid for such a vertex point with an acute angle if there is no material perpendicular to the crack front. This will not be discussed in detail here.

In the case of a/c=1 (Fig. 7a), the value for $Y(\chi = 90°)$ differs from $Y(\chi = 70°)$ in point A by about 10%, which is a noticeable effect and has also a direct impact on fracture toughness measurements. For $a/c = 0.4$ (see Fig. 7b), this influence is significantly lower with deviations of about 1.5% than for narrow crack (the same trend can be found in the uncertainty analysis in [17]).

4. Data fitting and discussion

To determine a generalized solution for $Y = Y(a/c,\ a/t,\ c/b,\ \phi,\ \nu,\ \chi)$ all its six parameters have to be regarded. Additionally, a fitting function derived from the data interpolation has to be accurate and easy to handle at the same time. NR fitted their results by a mainly engineering ansatz function and an empirical approach and the fitting formula is "easy to apply in practice". To begin with, the NRF is analyzed in terms of accuracy and expandability for the new parameters ν and χ.

4.1. Comparison of the results with the NRF

NR claim that their provided fitting function has a maximum error of ±5% [5] according to their FE results and their indicated fitting error always is related to the maximum along the crack front. In addition they specified their FE accuracy with ±3% compared to the analytical solution in terms of a completely embedded circular crack.[6,7] Because they used a relative coarse mesh, especially along the crack front, some detail got lost near the free surface. Due to this point and considering the error by data fitting – it is clear why their solution deviates from the results in this work. The maximum fitting error with respect to the current position along the crack front probably increases up to 10%. By adding other terms to fit two more parameters

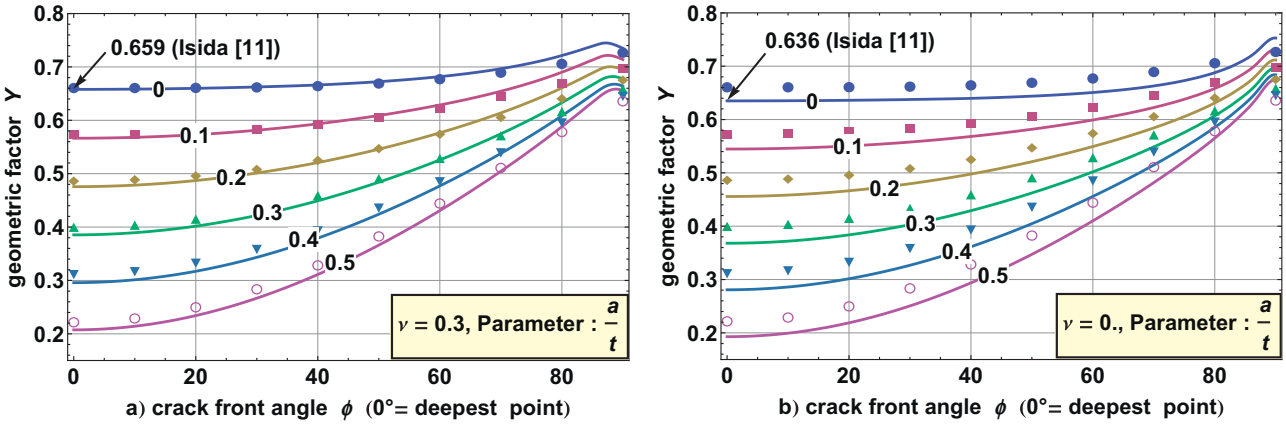

Fig. 4. Our FE results (lines) compared with the NRF (points) in the case of a semi-circular crack (a/c=1) along the crack front. Parameter in the curves is the relative crack depth a/t. (a) $\nu = 0.3$ and (b) $\nu = 0$.

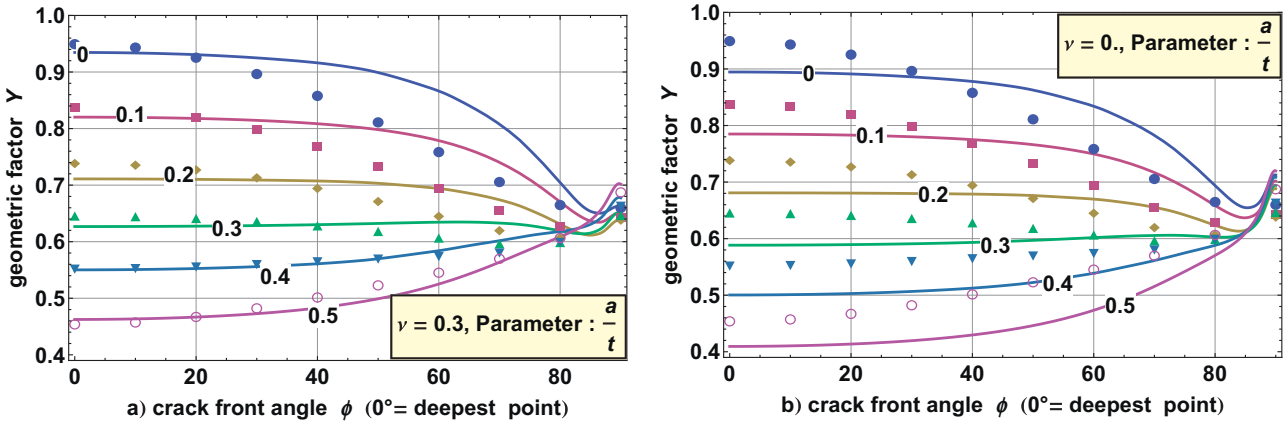

Fig. 5. Our FE results (lines) compared with the NRF (points) in the case of a shallow semi-elliptical crack ($a/c = 0.4$) along the crack front. Parameter in the curves is the relative crack depth a/t. (a) $\nu = 0.3$ and (b) $\nu = 0$.

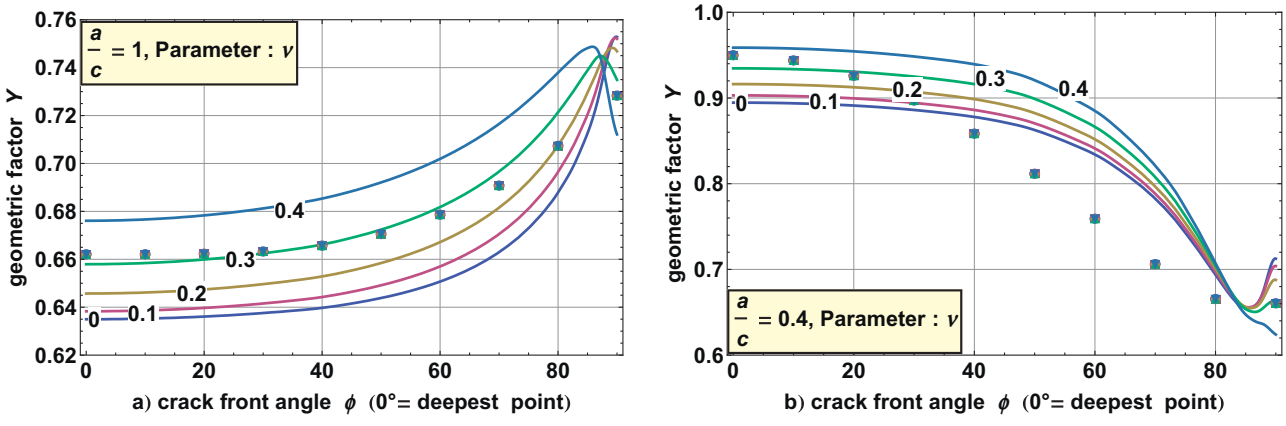

Fig. 6. Influence on Y of the Poisson's ratio ν plotted as parameter against ϕ ($a/t = 0$). The lines represent the actual FE study; the solution of NR (points) is independent from ν. (a) $a/c = 1$ and (b) $a/c = 0.4$.

would further increase the error and let the dimension of the fitting function blow up.

To determine the accuracy of the given NRF two examples for bending with $\nu = 0.3$, $c/b = 0.1$ and $\chi = 90^\circ$ are illustrated in Fig. 8. The NR solution within the intersecting parameter intervals fits the actual FE results quite good in point A (deviation maximum: 7.7%, average: 1.5%) and in point C (deviation maximum: 8.2%, average: 2.4%). But between those points, the maximum deviation rises up to about 13% (mean: 2.6%) – this worst (and relevant) case is given in Fig. 8a. Assuming other relative crack depths (see Fig. 8b) the general agreement is better, but the deviation is also for point A about

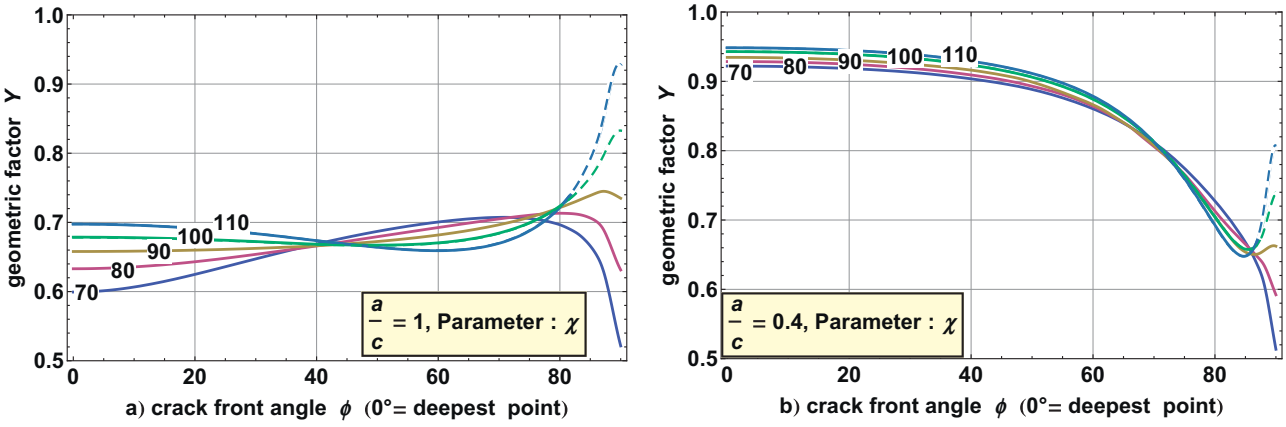

Fig. 7. Influence of the crack-surface interaction angle χ plotted as parameter against ϕ with $a/t = 0$ and $\nu = 0$. Subfigure (a) shows $a/c = 1$ and (b) $a/c = 0.4$.

10% ($a/c = 1.2$ and $\phi = 0°$). For tension the deviations are about the half of the bending case.

Because of these differences in Y, a new fitting function was created instead of additional (correction) term for NRF for $\nu \neq 0.3$ and $\chi \neq 90°$.

4.2. Practical aspects in terms of fracture toughness evaluation with the SCF-method

The surface crack in flexure (SCF) method is frequently used to determine the fracture toughness of ceramics.[5,24,25] A Knoop hardness indent is made on the tensile loaded side of a rectangular bending bar. The indent causes some plastic deformation around the intended zone, which also causes unknown internal stresses. They are relaxed by removing the plastic deformed material by grinding-off the surface layer of the specimen's surface which contains the plastically deformed zone. Thus, a crack with the shape of an ellipse section is introduced in the surface (Fig. 2). Size and geometry of the surface crack has to be determined by fractographic means (which may need some fractographic experience).

A representative example of a crack after grinding – used for the SCF-method – is illustrated in Fig. 9 for a silicon carbide ceramic. The crack is made visible using fluorescent penetration dye. All needed parameters (a, c and χ) can easily be determined with a commercial light microscope. Note that – in the actual case – the crack surface interaction angle χ is about 70°.

All assumed parameter intervals for this analysis (see Table 1) are realistic in terms of the practical feasibility of the SCF-method. The limits of the crack geometry parameter are mainly designated through a qualified indentation load (i.e. HK10) and concerning commercial structural ceramics.

The intersection angle χ was chosen as an input parameter (instead of the grinding depth Δt) because it is much easier to determine than Δt. Concerning that the SCF-method will be an important application area of the SIF of such type of surface cracks the approaches for fitting are focusing on pure bending as the main loading case.

4.3. Simplified approach for data fitting

In general, the stress singularity at the free surface (at point C) is not proportional to $r^{-1/2}$ (with r as the distance from the crack tip) according to Fett,[18] Hutar [26–28] and deMatos.[21] Strictly spoken, the K-concept is therefore not valid at point C and it can only be used as a rough approximation at the vertex point. This is even more important including the effect of the Poisson's ratio and the results also depend on the crack-surface intersection angle χ.

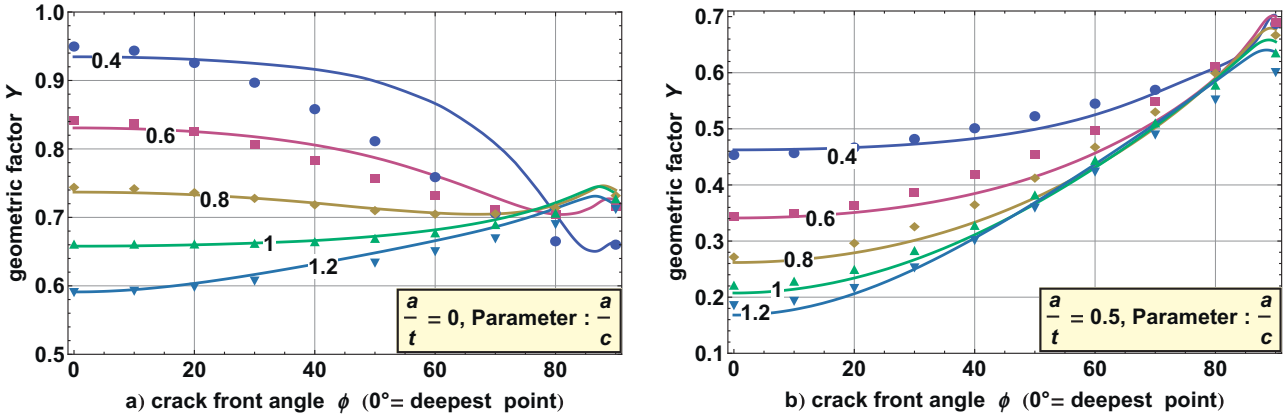

Fig. 8. Comparison of the solution for Y in bending of NR (points) and the actual FE results (lines) plotted against the crack front angle ϕ Parameter in the curves is the crack shape a/c. a) a/t=0 and b) a/t=0.5.

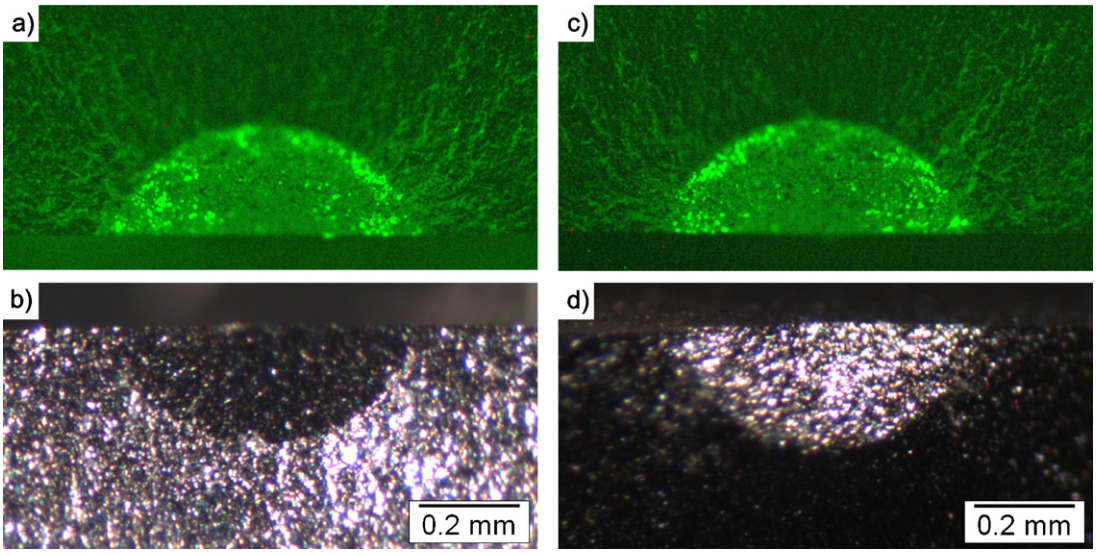

Fig. 9. Typical example of a Knoop crack in silicon carbide after removal of the plastic zone by grinding and after fracture. (a) and (c): visualisation of the crack by fluorescent penetration dye and UV-light. (b) and (d): conventional stereo microscopy. The crack-surface interaction angle χ is about 70°.

This twilight zone can be avoided by generating crack geometries, where $Y_A(\phi = 0^\circ)$ reaches its maximum value along the crack front. This guaranties the validity of fracture toughness evaluation for each specimen.

The value of the geometric function Y_A in the case of bending can be approximated by the fitting function in Eq. (4). The maximum fitting error is less than 2.7% and the average fitting error is about 0.4% (standard deviation: 0.3%). The geometric factor is:

$$Y\left(\frac{a}{c}, \frac{a}{t}, \frac{c}{b}, \nu, \chi, \phi = 0^\circ\right)_{\text{Bending}} = f \cdot f_b \cdot f_\nu \cdot f_\chi \tag{4}$$

with

$$f\left(\frac{a}{c}, \frac{a}{t}\right) = \left(1.11 + 1.71\left(\frac{a}{c}\right)^{1.42}\right)^{(-1/2)} \left(1.16 - 0.094\frac{a}{c} + \left(-1.67 + \frac{0.174}{0.256 + (a/c)}\right)\frac{a}{t} + \left(-0.09 - 0.045\left(1 - \frac{a}{c}\right) - \frac{-0.316}{0.14 + (a/c)}\right)\left(\frac{a}{t}\right)^2 - 0.186\left(\frac{a}{t}\right)^3\right) \tag{5}$$

and

$$f_b\left(\frac{a}{c}, \frac{a}{t}, \frac{c}{b}\right) = \cos\left(1.04\left(\frac{c}{b} - 0.1\right)\left(2\frac{a}{t}\right)^{0.5} 90^\circ\right)^{(-1/2)} \times \left(1 + \left(\frac{a}{c} - 0.41\right)\left(\frac{c}{b} - 0.1\right)\right) \times \left(-0.38\left(\frac{a}{c}\right)^2 + 1.4\right) \times \left(0.074 + 1.26\left(\frac{a}{t}\right)^3\right)\Bigg) \tag{6}$$

and

$$f_\nu\left(\frac{a}{c}, \frac{a}{t}, \nu\right) = \left(1 + 0.97\nu\left(-0.15\left(\frac{a}{c}\right) + 0.13\left(\frac{a}{c}\right)^2\right) \times \left(6.43\frac{a}{t} - 6.15\left(\frac{a}{t}\right)^{0.5}\right) \times + 0.68\nu^2\left(0.68 - 0.09\left(\frac{a}{c}\right)^2\right)\left(1 - 1.8\frac{a}{t} + 9.12\left(\frac{a}{t}\right)^2\right)\right) \tag{7}$$

and

$$f_\chi\left(\frac{a}{c}, \frac{a}{t}, \chi\right) = \left(1 - 0.31\left(\frac{a}{c}\right)^{1.7}\left(-1.46 - 4.25\left(\frac{a}{t}\right)^2\right) \times \left(1 - \left(\frac{90}{\chi}\right)^{0.72}\right)\right) \tag{8}$$

Additional terms to approximate the geometric factor along the whole crack front are given in Appendix A. The solution for the case of pure tension is treated in Appendix B.

To quantify the importance of consideration of the new parameters, the NRF ($\nu = 0.3$ and $\chi = 90^\circ$) and the new fit according to Eq. (4) is compared with the results of the actual FE study (interpolation) within the parameter range ($0 \le \nu \le 0.4$ and $70^\circ \le \chi = 90^\circ$) in the case of pure bending, see Table 2. For all other parameters the intersecting intervals have been chosen.

At this point it should clearly be said that the NRF was made for $\chi = 90^\circ$ and $\nu = 0.3$. But even for $\nu = 0.3$ and $\chi = 90^\circ$ the deviation rises up to 11% for both points A and C. In the worst case the deviations are about 50% which occur at $\nu = 0$ and $\chi = 70^\circ$ in both points. These extremely high deviations regarding the actual FE results are minor relevant for the SCF-method because they occur in point A only for almost semi-circular cracks for which Y_A is the minimum along the whole crack front.

Table 2
Maximum fitting error of the NRF and the fit according to Eq. (4) regarding the FE results (interpolation).

		Point A		Point C		Complete crack front	
		max.	mean	max.	mean	max.	mean
NRF							
$70° \le \chi \le 90°$	$0 \le \nu \le 0.4$	47.8%	7.7%	50.5%	14.8%	50.5%	5.0%
$70° \le \chi \le 90°$	$\nu = 0.3$	39.5%	5.4%	41.2%	15.8%	41.2%	4.4%
$\chi = 90°$	$0 \le \nu \le 0.4$	18.9%	4.2%	11.7%	4.4%	20.7%	4.0%
$\chi = 90°$	$\nu = 0.3$	11.4%	1.6%	10.9%	2.8%	13.8%	2.7%
Actual fit Eq. (4)							
$70° \le \chi \le 90°$	$0 \le \nu \le 0.4$	2.7%	0.4%	38.6%	11.1%	38.6%	4.0%
$70° \le \chi \le 90°$	$\nu = 0.3$	1.9%	0.4%	28.2%	11.4%	30.1%	4.0%
$\chi = 90°$	$0 \le \nu \le 0.4$	2.3%	0.3%	6.9%	2.3%	6.9%	1.0%
$\chi = 90°$	$\nu = 0.3$	1.8%	0.4%	5.8%	2.4%	6.7%	1.0%

The actual formula, given in Eq. (4), has a good agreement (max. 2.7% and 0.4% averaged) in point A in the complete field of the parameters which was the main purpose of this fit. With the assumption of $\chi = 90°$ the geometric factor can be calculated with a maximum deviation of 6.9% (mean: 1%) that is a tolerable fitting error. It is about the half compared to the NRF.

Considering Table 2 makes obvious that the new fitting function provides in every case a higher accuracy than the NRF even our equation is of similar length.

4.4. Evaluation of the minimum grinding depth

To get a valid K_{Ic} value also the ASTM standard for the SCF-method [24] instructs to use shallow crack shapes with $Y_{\mathrm{A}} > Y_{\mathrm{C}}$, i.e. the maximum of Y should be positioned at point A. In practice, the easiest way to realize this, is to increase the grinding depth Δt. But where is the critical grinding depth? It is not satisfying and a waste of time to see after testing and data evaluation that this sample has to be rejected. So what do one know about the specimen after indentation (before grinding): the original crack width $2c_0$ at the surface, the original thickness t_0 of the bar and an idea of the original crack shape a_0/c_0 (maybe approximated with $a_0/c_0 = 1$, from literature or determined in a pretest for the given material).

As can be seen from the results, Y_{A} as well as the maximum along the crack front Y_{Max} depend on the χ and ν. The Poisson's ratio is given for a specific material and χ is predetermined by the grinding depth, if you do serial sectioning to find the equilibrium depth, since Y_{A}=Y_{Max}. With this in mind one can calculate the critical grinding depth Δt related to c_0 with the FE results under tension and bending, that is illustrated in Fig. 10.

For ease of use, the relative grinding depth $\Delta t/c_0$ can be approximated for bending Eq. (9) and tension Eq. (10). The maximum fitting error for both solutions is less than 1.35% of c_0. This approximation takes also the Poisson's ratio as well as the initial crack shapes in the range $0.8 \le a_0/c_0 \le 1.2$ into account:

$$\frac{\Delta t}{c_0}\left(\frac{a_0}{c_0}, \frac{c_0}{t_0}, \nu\right)_{\mathrm{Bending}} = 0.493 + 1.28\left(\frac{a_0}{c_0} - 1\right) + 1.15\frac{c_0}{t_0} - 1.84\left(\frac{c_0}{t_0}\right)^2 + 3.43\left(\frac{a_0}{c_0}\right)^{0.4}\left(\frac{c_0}{t_0}\right)^4 + \left(1 - 0.88\frac{c_0}{t_0}\right)(-0.15\nu - 1.3\nu^2 + 1.73\nu^4) \quad (9)$$

and

$$\frac{\Delta t}{c_0}\left(\frac{a_0}{c_0}, \frac{c_0}{t_0}, \nu\right)_{\mathrm{Tension}} = 0.518 + 1.4\left(\frac{a_0}{c_0} - 1\right) - 0.152\frac{c_0}{t_0} + 0.84\left(\frac{c_0}{t_0}\right)^2 - 0.55\left(\frac{c_0}{t_0}\right)^3 + \left(-2.1 + \frac{c_0}{t_0}\right)(0.045\nu + 1.1\nu^2 - \nu^3) \quad (10)$$

To illustrate the significance of these findings a short example is presented. As material with a very low Poisson's ratio a

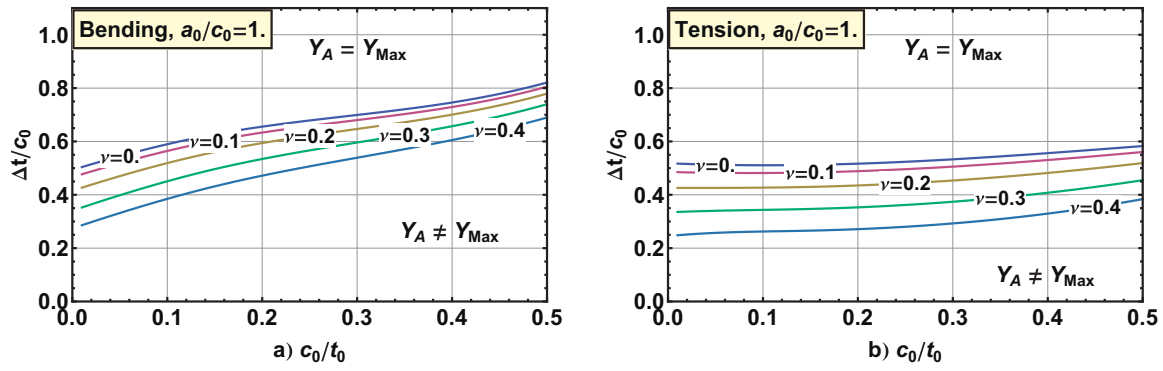

Fig. 10. Rel. grinding depth Δt plotted vs. the initial rel. crack width c_0 for an initial crack shape of $a_0/c_0 = 1$. Above the lines the maximum SIF occurs at the deepest point of the crack. Parameter is the Poisson's ratio. (a) bending and (b) tension case.

commercial silicon carbide was chosen with $\nu = 0.16$. A standard 4-point bending beam ($3 \times 4 \times 50\,mm^3$) was produced to carry out a fracture toughness test with the SCF-method with an indenter load of 4 kg (Knoop). After indentation, a surface layer of about 75 μm was removed (60 μm are suggested by Eq. (9) for $a_0/c_0 = 1$) to initiate the fracture at the deepest point of the crack. The specimen used for testing had the following geometry: $t = 2.853$ mm, $b = 2.001$ mm, $a = 57\,\mu m$, $c = 91\,\mu m$ and $\chi = 65°$. For this specimen the NRF results in geometric factors of $Y_A = 0.808$ and $Y_C = 0.716$. The actual interpolation function provides the values $Y_A = 0.737$ and $Y_C = 0.526$, respectively. In both cases point A has the highest value of Y along the whole crack front; however, the results of the formulas differ significantly. Considering the influence of the Poisson's ratio and the crack-surface intersection angle allows a difference of Y_A of about 8.8% to be obtained. Furthermore, the supported fitting formula provides in point A $Y_A = 0.730$ instead of 0.737 which encompasses a fitting error of about 1%.

5. Concluding remarks

The geometry factor Y was calculated within a practical range of crack and specimen geometries by FEA. These results are compared with the Newman and Raju formula.

The developed interpolation function of the new results takes also the Poisson's ratio and the crack-surface interaction angle into account, which has a significant influence on the geometric factor. If the crack aspect ratio a/c is low enough, the deepest point of the crack gets critical; this is a well-defined situation in fracture mechanics. Hence, fitting functions for the geometric factor Y in tension and bending have been developed for this specific case considering the new parameters.

The influence of the surface-crack interaction angle on Y_A is high for almost semi-circular cracks but decrease with decreasing crack shape ratios a/c.

The implications for fracture toughness measurements using SCF-methods are discussed. The above argument indicates to aim shallow cracks for fracture toughness measurement with the SCF-method. Also the critical grinding depth Δt was calculated to guarantee that Y_A becomes the maximum. An approximate formula for the grinding depth is given regarding pre-known quantities. This simplifies, among other things, the practical usage of the standardized SCF-method for a (scientific) determination of the fracture toughness.

Acknowledgements

Financial support by the Austrian Federal Government (in particular from the Bundesministerium für Verkehr, Innovation und Technologie and the Bundesministerium für Wirtschaft, Familie und Jugend) and the Styrian Provincial Government, represented by Österreichische Forschungsförderungsgesellschaft mbH and by Steirische Wirtschaftsförderungsgesellschaft mbH, within the research activities of the K2 Competence Centre on "Integrated Research in Materials, Processing and Product Engineering", operated by the Material Center Leoben Forschung GmbH in the framework of the Austrian COMET Competence Centre Programme, is gratefully acknowledged.

Appendix A. Fit function for Y along the crack front under bending load

The results of the FEM-calculations for Y along the complete crack front in the case of bending can be approximated by Eq. (A.1) with a maximum fitting error of 6.7% and an average fitting error of 0.9% (standard deviation: 1%). The only restriction for this fit along the crack front is χ=90°. Note that f_ϕ reduces to 1 in the case ϕ=0° (i.e. in point A).

$$Y\left(\frac{a}{c}, \frac{a}{t}, \frac{c}{b}, \nu, \chi = 90°, \phi\right)_{\text{Bending}} = f \cdot f_b \cdot f_\nu \cdot f_\chi \cdot f_\phi \tag{A.1}$$

$$\begin{aligned} f_\phi\left(\frac{a}{c}, \frac{a}{t}, \frac{c}{b}, \nu, \phi\right) = {} & \left(\left(\frac{a}{c}\right)^2 \sin(\phi)^2 + \cos(\phi)^2\right)^{1/4} \cdot \\ & \left(1 + \left(0.11\left(1.9 - \frac{a}{c}\right)\left(1 + \frac{a}{t}\right) - 0.02/\left(\frac{a}{c}\right)\sin\left(\frac{a}{t}360\right)\right)\left(1 + 11\nu\left(\frac{a}{t}\right)^6\left(0.11 - \left(0.13 - \frac{a}{t}\right)^2\right)\right)\right. \\ & \left(\frac{\phi}{90}\right)^3 + 0.05(1 - 3.7\nu)\left(\frac{\phi}{90}\right)^{10} + 0.085/\left(\frac{a}{c}\right)(1 - 2.3\nu)\left(\frac{\phi}{90}\right)^{20} - 0.05/\left(\frac{a}{c}\right)\left(\frac{\phi}{90}\right)^{50}\Bigg) \\ & \left(1 + \left(0.28\left(2\frac{a}{t}\right)^{0.9} + 0.72\left(2\frac{a}{t}\right)^{\left(1+2.3\frac{a}{c}\right)}\right)\left(0.69\left(\frac{a}{t} + 0.25\right)\right)\right. \\ & \left.\left(\left(2.15 - 0.28\frac{c}{b}\right)\left(\left(\frac{\phi}{90}\right)^{\left(3.9-1.99\frac{a}{t}\right)} + \left(\frac{\phi}{90}\right)^3\left(1 - \frac{\phi}{90}\right)\right)\right)\right) \\ & \left(1 + 1.8\left(1 - \frac{\phi}{90}\right)\left(\left(-0.54\nu + 0.07\frac{c}{b}\right)\left(\frac{\phi}{90}\right)^6 + \left(1 - 2\frac{a}{t}\right)\right.\right. \\ & \left.\left.\left(\left(1.2 - \frac{a}{t}\right)/0.8\right)^4 0.7\left(\frac{\phi}{90}\right)^{2.5} - 3\left(\left(1.2 - \frac{a}{t}\right)/0.8\right)\exp\left[-19.5\left(1 - \frac{\phi}{90}\right)\right]\right)\right) \end{aligned} \tag{A.2}$$

Appendix B. Fit function for Y along the crack front in pure tension

The numerical values of the geometric factor Y in the case of tension can be approximated by Eq. (B.1). This equation fits the FE results within a maximum error of 1% (average: 0.21%) for point A. Along the whole crack front – with the restriction χ=90°– the maximum fitting error is 2.6% (average: 0.36%). Note that $f_{\phi,\mathrm{T}}$ reduces to 1 in the case ϕ=0° (i.e. in point A).

$$Y\left(\frac{a}{c},\frac{a}{t},\frac{c}{b},\nu,\chi,\phi\right)_{\text{Tension}} = f_T \cdot f_{b,T} \cdot f_{\nu,T} \cdot f_{\chi,T} \cdot f_{\phi,T} \tag{B.1}$$

$$f_T\left(\frac{a}{c},\frac{a}{t}\right) = \left(0.864 + 1.626\left(\frac{a}{c}\right)^{1.57}\right)^{-1/2} \times \left(1 + \left(0.027 + 0.01/\left(\frac{a}{c}\right)\right)\frac{a}{t} + (-0.3 - 0.116\left(1 - \frac{a}{c}\right) + 0.415/\left(\frac{a}{c}\right)\right)\left(\frac{a}{t}\right)^{2.3}\right) \tag{B.2}$$

$$f_{b,T}\left(\frac{a}{c},\frac{a}{t},\frac{c}{b}\right) = 1 + 0.0105\frac{a}{c}\left(\frac{c}{b} + 25.7\left(\frac{c}{b}\right)^4\right) \times \left(1 + 118\left(0.08 - \left(\frac{c}{b} - 0.36\right)^2\right) \times \left(\frac{a}{t} - 0.14\left(2\frac{a}{t}\right)^{10}\right)/\left(\frac{a}{c}\right)\right) \tag{B.3}$$

$$f_{\nu,T}\left(\frac{a}{c},\frac{a}{t},\nu\right) = \left(1 + 0.77\nu\left(\left(\frac{a}{c}\right)^{0.5} - 1\right) \times \left(-0.16 - \left(\frac{a}{t}\right)^2\right) + \nu^2\left(-0.1 - 0.225\frac{a}{c} + 0.39\left(\frac{a}{c}\right)^{0.5}\right)\left(6.31 + 3.4\frac{a}{t} - 1.2\left(\frac{a}{t}\right)^{0.5}\right)\right) \tag{B.4}$$

$$f_{\chi,T}\left(\frac{a}{c},\frac{a}{t},\frac{c}{b},\chi\right) = \left(1 + 0.44\left(1 + 0.33\left(\frac{c}{b}\right)^2\right)\left(\frac{a}{c}\right)^{1.9} \times \left(1 - \left(\frac{90}{\chi}\right)^{0.7}\right) - 0.004(90 - \chi)\left(\frac{a}{t}\left(\frac{c}{b}\right)^3 + 0.22\frac{a}{t}\right)\right) \tag{B.5}$$

$$f_{\phi,T}\left(\frac{a}{c},\frac{a}{t},\frac{c}{b},\nu,\phi\right) = \left(\left(\frac{a}{c}\right)^2\sin(\phi)^2 + \cos(\phi)^2\right)^{1/4} \left(1 + 0.056\left(\frac{\phi}{90}\right)^2 + 0.12\left(\frac{a}{c}\right)^{-0.9}\left(1 - 3\left(1 - \frac{a}{c}\right)^5\right)\left(\frac{\phi}{90}\right)^{(5+4(a/c))}\right) \left(1 + 0.24\left(\frac{a}{t}\right)^3/\left(\frac{a}{c}\right)\left(\frac{\phi}{90}\right)^3 + 0.96\left(\frac{a}{t}\right)^2\left(\frac{c}{b} - 0.1\right)\left(\frac{a}{c}\right)^{0.5}\left(\frac{\phi}{90}\right)^2\right) \left(1 + 0.32\,\nu\left(\left(\frac{a}{c} - 0.8\right) + 0.45\frac{a}{t}\left(1 - 1.6\frac{c}{b}\right)\right)\left(\frac{\phi}{90}\right)^{2.5} - 0.136\left(\frac{\nu}{0.4}\right)^2\left(\frac{\phi}{90}\right)^{(25(a/c))}\right) \tag{B.6}$$

References

1. Lawn BR. *Fracture of brittle solids*. 2nd ed. Cambridge: Cambridge University Press; 1993.
2. Munz D, Fett T. *Ceramics – mechanical properties, failure behaviour, materials selection*. Berlin: Springer; 2001.
3. Fett T, Munz D. *Stress intensity factors and weight functions*. Southampton UK and Boston USA: Computational Mechanics Publications; 1997.
4. Murakami Y. *Stress intensity factors handbook*. Oxford: Pergamon Press; 1987-2001.
5. Newman JC, Raju IS. An empirical stress-intensity factor equation for the surface crack. *Engineering Fracture Mechanics* 1981;**15**:185–92.
6. Raju IS, Newman JC. Improved stress-intensity factors for semi-elliptical surface cracks in finite-thickness plates. NASA Report TM-X-72825; 1977.
7. Newman JC, Raju IS. Analysis of srface cracks in finite plates under tension or bending loads. NASA. Report TP-1578; 1979.
8. Shackelford JF. *CRC materials science and engineering handbook*. Boca Raton, FL: CRC Press; 1994.
9. Field JE. *Properties of natural and synthetic diamond*. London: Academic Press; 1992.
10. Czichos H, Hennecke M. *Hütte – Das Ingenieurwissen*. Berlin Heidelberg: Springer; 2008.
11. Isida M, Noguchi H, Yoshida T. Tension and bending of finite thickness plates with a semi-elliptical surface crack. *International Journal of Fracture* 1984;**26**:157–88.
12. McGowan JJ. *A critical evaluation of numerical solutions to the benchmark surface flaw problem*. Westport: Society for Experimental Stress Analysis; 1980.
13. Newman JC. A review and assessment of the stress intensity factor for surface cracks. Chang JB, editor. *Part-through crack fatigue life prediction, ASTM STP 687*. American Society for Testing and Materials; 1979.
14. Smith FW. The elastic analysis of part-circular surface flaw problems by the alternation method. Chang JB, editor. *The surface crack: physical problems and computational solutions*. New York: American Society of Mechanical Engineers; 1972.
15. Smith FW, Alavi MJ. Stress intensity factors for a part-circular surface flaw. In: *1st international pressure vessel conference*. 1969. p. 793–800.
16. Quinn GD, Gettings RJ, Kübler J. Fracture toughness by the surface crack in flexure (SCF) method: results of the VAMAS Round Robin. *Ceramic Engineering and Science Proceedings* 1994;**15**:846–55.
17. Quinn GD, Kübler J, Gettings RJ. Fracture toughness of advanced ceramics by the surface crack in flexure (SCF) method: a VAMAS Round Robin. VAMAS Report No. 17. Report 1994.
18. Fett T. *Stress intensity factors – T-stresses – weight functions. Supplement volume (IKM 55)*. Karlsruhe: KIT Scientific Publishing; 2009.
19. Anderson TL. *Fracture mechanics – fundamentals and applications*. Boca Raton FL: CRC Press; 2005.
20. Courtin S, Gardin C, Bézine G, Ben Hadj Hamouda H. Advantages of the J-integral approach for calculating stress intensity factors when using the commercial finite element software ABAQUS. *Engineering Fracture Mechanics* 2005;**72**:2174–85.
21. de Matos PFP, Nowell D. The influence of the Poisson's ratio and corner point singularities in three-dimensional plasticity-induced fatigue crack closure: a numerical study. *International Journal of Fatigue* 2008;**30**:1930–43.

22. Zúñiga DF, Kalthoff JF, Canteli AF, Grasa J, Doblaré M. Three dimensional effects along the crack front influencing the validity criteria for determining fracture toughnesses. 11th International Conference on Fracture, Turin (Italy): 2005.
23. Fett T. Stress intensity factors for semi-elliptical surface cracks in a plate under tension based on the Isida's solution. *International Journal of Fracture* 1991;**48**:139–51.
24. ASTM C 1421-01b. *Standard test methods for determination of fracture toughness of advanced ceramics at ambient temperature*. American Society for Testing and Materials; 2001.
25. ISO 18756. *Fine ceramics (advanced ceramics, advanced technical ceramics) – determination of fracture toughness of monolithic ceramics at room temperature by the surface crack in flexure (SCF) method*; 2003.
26. Hutar P, Náhlík L, Knésl Z. Quantification of the influence of vertex singularities on fatigue crack behavior. *Computational Materials Science* 2009;**45**:653–7.
27. Hutar P, Náhlík L, Knésl Z. The effect of a free surface on fatigue crack behaviour. *International Journal of Fatigue* 2010;**32**:1265–9.
28. Hutar P, Sevcík M, Náhlík L, Zouhar M, Seitl S, Knésl Z, et al. Fracture mechanics of the three-dimensional crack front: vertex singularity versus out of plain constraint descriptions. *Procedia Engineering* 2010;**2**:2095–102.